ISSN 0030-400X, Optics and Spectroscopy, 2015, Vol. 119, No. 3, pp. 411–423. © Pleiades Publishing, Ltd., 2015.

SPECTROSCOPY OF ATOMS AND MOLECULES

Theoretical (DFT) and Experimental (FT-IR, FT-Raman, FT-NMR) Investigations on 7-Acetoxy-4-(Bromomethyl)Coumarin[1]

Y. Erdogdu[a], S. Saglam[b], and Ö. Dereli[c]

[a] *Department of Physics, Ahi Evran University, 40040 Kirsehir, Turkey*

[b] *Department of Physics, Gazi University, 06100 Ankara, Turkey*

[c] *Department of Physics, Necmettin Erbakan University, Meram, 42090 Konya, Turkey*

e-mail: yusuferdogdu@gmail.com

Received February 2, 2015

Abstract—An analysis of the results of the structural and spectroscopic studies of 7-Acetoxy-4-(bromomethyl)coumarin (7A4BMC) molecule were performed by FT-IR, FT-Raman, FT-NMR and quantum chemical calculations. The FT-IR and FT-Raman spectra of 7A4BMC were recorded in the 400–4000 and 50–3500 cm^{-1} region, respectively. The molecular conformations of 7A4BMC were computed at the B3LYP/6-311++G(d,p) level of theory. Molecular structure and spectral calculations were calculated by means of B3LYP with 6-311++G(d,p), cc-pVDZ and cc-pVTZ basis sets. The whole vibrational characteristics of the 7A4BMC molecule are given.

DOI: 10.1134/S0030400X15090076

1. INTRODUCTION

It has been clearly stated by Ranjith et al. [1] and Sidir et al. [2] that during the last few years, there has been a remarkable growth in the use of fluorescence in biological sciences especially in biochemistry and biophysics. Fluorescence also finds application in environmental monitoring, clinical chemistry, DNA sequencing and genetic analysis by fluorescence in situ hybridization (FISH). In molecular biology, fluorescence is used for cell identification and sorting in flow cytometry, and in cellular imaging to reveal the localization and movement of intracellular substances by means of fluorescence microscopy. Because of the high sensitivity of fluorescence detection, there is continuing development of medical tests based on the phenomenon of fluorescence. These tests include the widely used enzyme linked immunoassays (ELISA) and fluorescence polarization immunoassays [1]. Coumarins, which are organic laser dyes, have many applications. The widespread of these compounds have been used as fluorescence derivatization reagents for high-performance liquid chromatography [3], fluorescence probes for protein studies [4], fluorescent ionophores [5] and fluorescent indicators [6]. As they are highly fluorescent molecules, coumarins has been also the subject of photophysical studies during the last few decades.

Recently, spectroscopic investigations supported by DFT computations on some coumarin derivatives have been carried out by many researchers [7–14]. Taking into account the bromomethyl coumarin and acetoxy coumarin derivatives, Sortur and co-workers reported the vibrational spectral investigations of 6-methyl and 7-methyl-4-bromomethylcoumarin [15, 16]. For 6-Chloro and 7-Chloro-4-bromomethylcoumarins, similar studies were performed by Tonannavar et al. [17]. Density functional theory study of FT-IR and FT-Raman spectra of 7-acetoxy-4-methylcoumarin molecules was also reported by Arivazgahan et al. [18]. In addition to all these, we reported the vibrational spectroscopic studies on the 3-(bromoacetyl)coumarin by theoretical (DFT) and experimental methods (FT-IR, FT-Raman and NMR spectra) [19].

To the best of our literature knowledge, DFT calculations and experimental studies on vibrational spectra of 7A4BMC molecule have not been reported so far. Therefore, we have carried out detailed theoretical and experimental investigation on the vibrational spectra of 7A4BMC completely. We have utilized DFT/B3LYP with 6-311++G(d,p), cc-pVDZ and cc-pVTZ basis sets [20–22].

2. EXPERIMENTAL

2.1. Fourier-Transform Infrared Spectroscopy

The FT-IR spectrum of 7A4BMC was recorded in the region 400–4000 cm^{-1} on IFS 66V spectrophotometer using KBr pellet technique is shown in Fig. 1. The spectral resolution is ± 2 cm^{-1}.

[1] The article is published in the original.

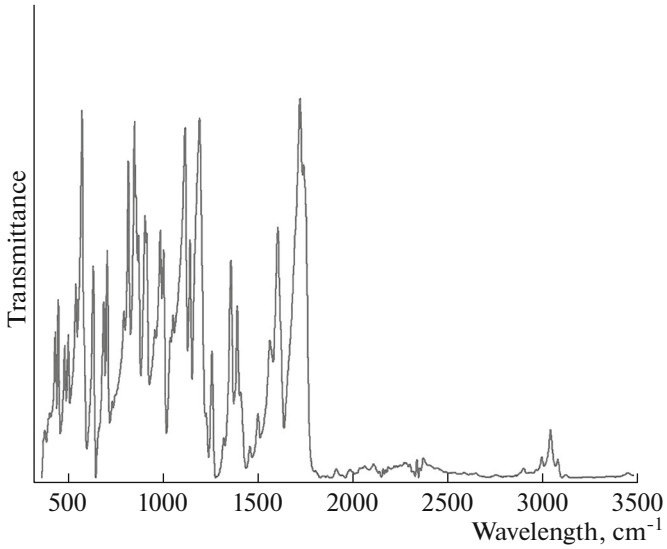

Fig. 1. Experimental FT-IR spectra of 7-Acetoxy-4-(bromomethyl)coumarin compound.

2.2. Fourier-Transform Raman Spectroscopy

The FT-Raman spectrum of 7A4BMC was recorded using 1064 nm line of Nd: YAG laser as excitation wavelength in the region 50–3500 cm^{-1} on Bruker FRA 106/S and shown in Fig. 2. The spectra were recorded with scanning speed of 30 cm^{-1} min^{-1} of spectral width 2 cm^{-1}. The frequencies of all sharp bands were accurate to ±1 cm^{-1}.

2.3. Fourier-Transform NMR Spectroscopy

The ^{13}C NMR spectra were taken in chloroform solutions. All signals were referenced to TMS on a Bruker superconducting FT-NMR spectrometer. The NMR spectra was measured at room temperature.

3. COMPUTATIONAL DETAILS

In order to establish the stable possible conformations, the conformational space of 7A4BMC molecule was scanned with molecular mechanic simulations. Rotating 10 each degree intervals around the free rotation bonds, conformational space of the 7A4BMC molecule was scanned by molecular mechanic simulations. This calculation was performed with the Spartan 10 program [23]. Full geometry optimizations of all possible candidate structures were performed by B3LYP/6-311++G(d,p) method. The full optimizations calculations were performed at DFT levels by using Gaussian 09 [24, 25] program.

In the present work, the DFT/B3LYP functional with 6-311++G(d,p), cc-pVDZ and cc-pVTZ basis sets were used for optimization, molecular structure, vibrational and NMR spectra. The vibrational modes were assigned on the basis of TED analysis for B3LYP/6-311++G(d,p), using SQM program [26]. Only TED components ⩾10% was considered to perform the final assignment. It should be noted that Gaussian 09 program does not calculate the Raman intensities. Gaussian 09 calculates the Raman scattering activities. So, the Raman activities were converted to Raman intensities by means of RaInt program [27].

NMR analysis has been done by using gauge independent atomic orbital (GIAO) method. The ^{13}C NMR spectra calculations were performed by Gaussian 09 program package. The ^{13}C NMR chemical shifts calculations of the most stable conformer of the 7A4BMC molecule were made by using B3LYP functional with 6-311++G(d,p) basis set. The calculations

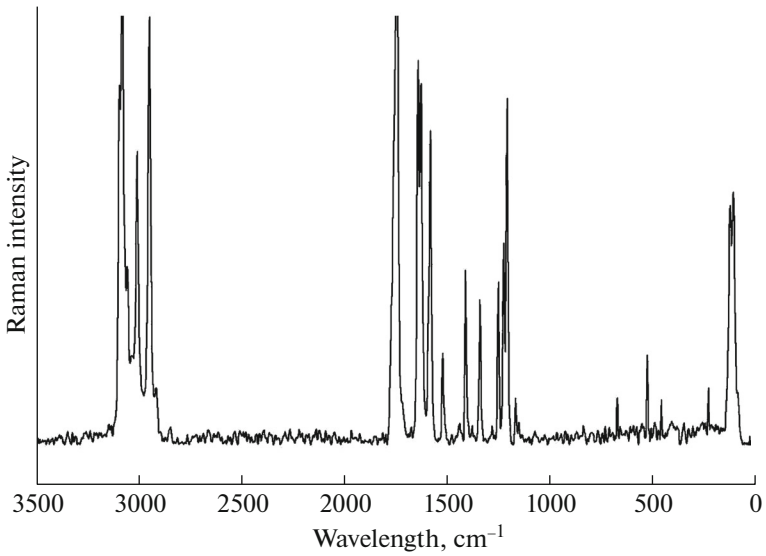

Fig. 2. Experimental FT-Raman spectra of 7-Acetoxy-4-(bromomethyl)coumarin compound.

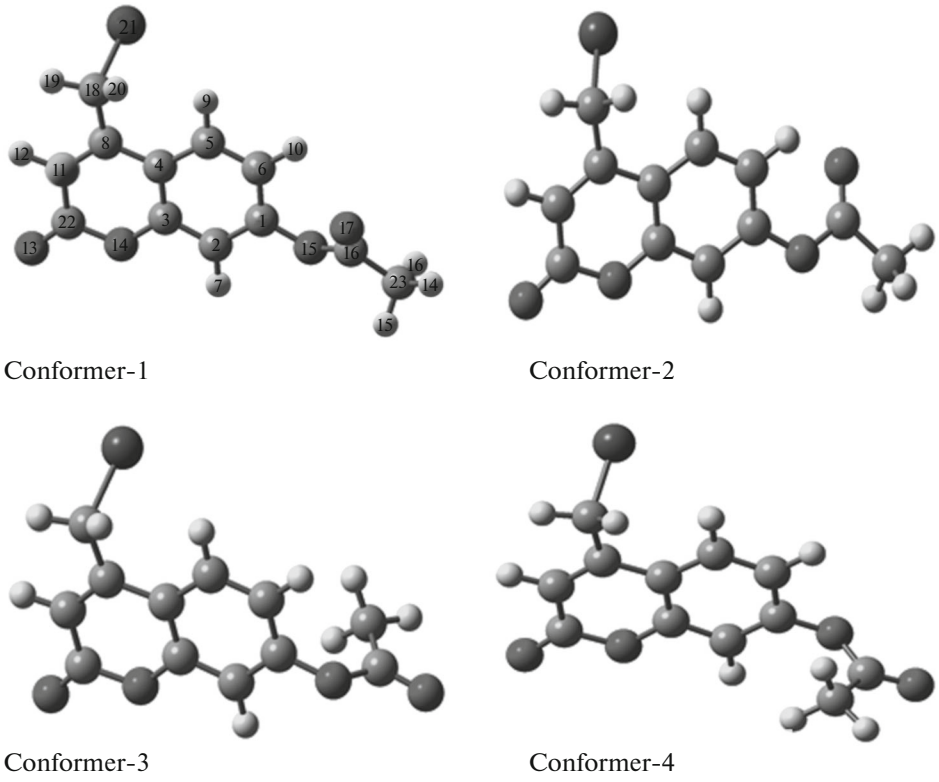

Fig. 3. All conformers and atomic numbering of 7-Acetoxy-4-(bromomethyl)coumarin compound.

were performed in chloroform solution by using IEF-PCM model. Results compared with experimental results for the identification and characterization of 7A4BMC molecule.

In order to correlate electro negativity and sites of chemical reactivity of the molecule, electrostatic potential surface has been plotted. The natural bonding orbital (NBO) analysis has been performed in order to investigate intra-molecular charge transfer interactions, rehybridization and delocalization of electron density within the molecule.

Table 1. Energetic of the four conformers calculated at the B3LYP/6-311++G(d,p) level

Conformers	E, Hartree	ΔE, kcal/mol	ΔE_0, kcal/mol
Conformer-1	–3335.33332627	0.000	0.000
Conformer-2	–3335.33307917	0.155	0.184
Conformer-3	–3335.32523260	5.078	4.971
Conformer-4	–3335.32493078	5.268	5.165

E_0—zero-point corrected energy.

4. RESULTS AND DISCUSSION

4.1. Conformational Analysis

Results of conformational analysis indicated that the 7A4BMC molecule is rather flexible molecule, may have at least four conformers as shown in Fig. 3. The numbering scheme for 7A4BMC is shown in Fig. 3. Optimized bond parameters were calculated by using B3LYP with 6-311++G(d,p) basis set. Ground state energies, zero point corrected energies ($E_{\text{elect.}}$ + ZPE), relative energies and dipole moments of conformers were presented in Table 1. Zero point corrections have not caused any significant changes in the stability order. Optimized geometric parameters are listed in Table 2.

4.2. Vibrational Assignments

The observed and calculated vibrational frequencies along with assignments have been summarized in Table 3. The calculations of vibrational spectral were performed using the Gaussian 09 [24] program package. These results were obtained using the B3LYP functional with the 6-311++G(d,p), cc-pVDZ and cc-pVTZ basis sets. The 7A4BMC molecule possess to C_1 point group symmetry. The 7A4BMC molecule consists of 26 atoms. It has 72 vibrational modes, all of which are active in the infrared and Raman spectra.

Table 2. Optimized geometric parameters of 7A4BMC compound

Bond lengths, Å	B3LYP/6-311++G(d,p)	B3LYP/cc-pVDZ	B3LYP/cc-pVTZ
C_1–C_2	1.384	1.395	1.382
C_1–C_6	1.398	1.406	1.395
C_1–O_{15}	1.389	1.387	1.386
C_2–C_3	1.392	1.393	1.388
C_2–H_7	1.081	1.089	1.079
C_3–C_4	1.406	1.412	1.403
C_3–O_{14}	1.363	1.363	1.360
C_4–C_5	1.407	1.408	1.403
C_4–C_8	1.452	1.454	1.448
C_5–C_6	1.383	1.390	1.379
C_5–H_9	1.082	1.090	1.079
C_6–H_{10}	1.080	1.084	1.077
C_8–C_{11}	1.355	1.360	1.351
C_8–C_{18}	1.495	1.497	1.492
C_{11}–H_{12}	1.082	1.090	1.080
C_{11}–C_{22}	1.455	1.458	1.452
O_{13}–C_{22}	1.202	1.205	1.200
O_{14}–C_{22}	1.392	1.396	1.390
O_{15}–C_{16}	1.379	1.376	1.375
C_{16}–O_{17}	1.198	1.204	1.196
C_{16}–C_{23}	1.503	1.506	1.501
C_{18}–H_{19}	1.085	1.094	1.082
C_{18}–H_{20}	1.086	1.096	1.084
C_{18}–Br_{21}	1.994	1.993	1.988
C_{23}–H_{24}	1.087	1.096	1.085
C_{23}–H_{25}	1.092	1.100	1.089
C_{23}–H_{26}	1.092	1.100	1.090

Bond angles, degrees	B3LYP/6-311++G(d,p)	B3LYP/cc-pVDZ	B3LYP/cc-pVTZ
C_2–C_1–C_6	121.4	120.8	121.3
C_2–C_1–O_{15}	116.3	113.0	116.1
C_6–C_1–O_{15}	122.0	126.1	122.4
C_1–C_2–C_3	118.7	119.5	118.9
C_1–C_2–H_7	121.1	120.5	121.0
C_3–C_2–H_7	120.1	119.9	120.0
C_2–C_3–C_4	121.6	121.3	121.5
C_2–C_3–O_{14}	116.3	116.3	116.4
C_4–C_3–O_{14}	122.0	122.2	122.0
C_3–C_4–C_5	117.6	117.4	117.6
C_3–C_4–C_8	117.4	117.4	117.4
C_5–C_4–C_8	124.8	125.0	124.8
C_4–C_5–C_6	121.5	122.2	121.6
C_6–C_5–H_9	119.6	119.5	119.6
C_6–C_5–H_9	118.7	118.1	118.7
C_1–C_6–C_5	118.9	118.5	118.9
C_1–C_6–H_{10}	120.4	120.5	120.4
C_5–C_6–H_{10}	120.6	120.9	120.6
C_4–C_8–C_{11}	119.2	119.0	119.2
C_4–C_8–C_{18}	121.2	121.3	121.2
C_{11}–C_8–C_{18}	119.4	119.6	119.4
C_8–C_{11}–H_{12}	122.0	122.0	121.8
C_8–C_{11}–C_{22}	122.9	123.0	122.9
H_{12}–C_{11}–C_{22}	115.0	114.9	115.1
C_3–O_{14}–C_{22}	122.4	122.1	122.4
C_1–O_{15}–C_{16}	120.6	125.2	121.0
O_{15}–C_{16}–O_{17}	123.6	125.0	123.9
O_{15}–C_{16}–C_{23}	109.6	108.8	109.5
O_{17}–C_{16}–C_{23}	126.7	126.0	126.4
C_8–C_{18}–H_{19}	111.5	111.6	111.6
C_8–C_{18}–H_{20}	112.8	112.7	112.9
C_8–C_{18}–Br_{21}	112.0	112.0	112.0
H_{19}–C_{18}–H_{20}	110.0	109.9	109.9
H_{19}–C_{18}–Br_{21}	104.9	105.0	104.9
H_{20}–C_{18}–Br_{21}	104.9	104.9	104.9
C_{11}–C_{22}–O_{13}	126.0	126.0	126.0
C_{11}–C_{22}–O_{14}	115.8	116.0	115.8
O_{13}–C_{22}–O_{14}	118.0	117.8	118.0
C_{16}–C_{23}–H_{24}	109.3	109.3	109.3
C_{16}–C_{23}–H_{25}	109.8	109.9	109.9
C_{16}–C_{23}–H_{26}	109.9	109.8	109.9
H_{24}–C_{23}–H_{25}	110.0	110.2	110.1
H_{24}–C_{23}–H_{26}	110.1	110.2	110.1
H_{25}–C_{23}–H_{26}	107.4	107.2	107.3

Dihedral angles, degrees	B3LYP/6-311++G(d,p)	B3LYP/cc-pVDZ	B3LYP/cc-pVTZ
C_6–C_1–C_2–C_3	–0.414	–0.117	–0.328
C_6–C_1–C_2–H_7	179.4	179.82	179.41
O_{15}–C_1–C_2–C_3	–176.3	–179.4	–176.3
O_{15}–C_1–C_2–H_7	3.451	0.5357	3.4344
C_2–C_1–C_6–C_5	0.601	0.1123	0.4861
C_2–C_1–C_6–H_{10}	–179.7	–179.8	–179.9
O_{15}–C_1–C_6–C_5	176.3	179.30	176.20
O_{15}–C_1–C_6–H_{10}	–4.056	–0.633	–4.192
C_2–C_1–O_{15}–C_{16}	–130.3	–175.4	–134.0

Table 2. (Contd.)

Dihedral angles, degrees	B3LYP/6-311++G(d,p)	B3LYP/cc-pVDZ	B3LYP/cc-pVTZ	Dihedral angles, degrees	B3LYP/6-311++G(d,p)	B3LYP/cc-pVDZ	B3LYP/cc-pVTZ
$C_6–C_1–O_{15}–C_{16}$	53.71	5.2911	49.977	$C_4–C_8–C_{11}–C_{22}$	−0.404	0.0201	−0.353
$C_1–C_2–C_3–C_4$	−0.157	−0.116	−0.242	$C_{18}–C_8–C_{11}–H_{12}$	1.641	1.5449	1.5164
$C_1–C_2–C_3–O_{14}$	−179.9	−179.9	−179.9	$C_{18}–C_8–C_{11}–C_{22}$	−178.5	−178.3	−178.6
$H_7–C_2–C_3–C_4$	−179.9	179.93	−179.9	$C_4–C_8–C_{18}–H_{19}$	−165.4	−166.2	−165.5
$H_7–C_2–C_3–O_{14}$	0.211	0.1003	0.2906	$C_4–C_8–C_{18}–H_{20}$	−41.06	−41.90	−41.02
$C_2–C_3–C_4–C_5$	0.521	0.342	0.6277	$C_4–C_8–C_{18}–Br_{21}$	77.14	76.293	77.158
$C_2–C_3–C_4–C_8$	−178.9	−179.2	−179.0	$C_{11}–C_8–C_{18}–H_{19}$	12.61	12.138	12.673
$O_{14}–C_3–C_4–C_5$	−179.6	−179.8	−179.6	$C_{11}–C_8–C_{18}–H_{20}$	137.0	136.46	137.18
$O_{14}–C_3–C_4–C_8$	0.832	0.615	0.6888	$C_{11}–C_8–C_{18}–Br_{21}$	−104.7	−105.3	−104.6
$C_2–C_3–O_{14}–C_{22}$	179.2	179.63	179.26	$C_8–C_{11}–C_{22}–O_{13}$	−179.5	−179.8	−179.6
$C_4–C_3–O_{14}–C_{22}$	−0.556	−0.196	−0.453	$C_8–C_{11}–C_{22}–O_{14}$	0.684	0.3937	0.5901
$C_3–C_4–C_5–C_6$	−0.330	−0.350	−0.465	$H_{12}–C_{11}–C_{22}–O_{13}$	0.307	0.1917	0.2714
$C_3–C_4–C_5–H_9$	178.5	178.54	178.53	$H_{12}–C_{11}–C_{22}–O_{14}$	−179.4	−179.5	−179.5
$C_8–C_4–C_5–C_6$	179.0	179.16	179.14	$C_3–O_{14}–C_{22}–C_{11}$	−0.199	−0.307	−0.181
$C_8–C_4–C_5–H_9$	−2.033	−1.937	−1.848	$C_3–O_{14}–C_{22}–O_{13}$	179.9	179.93	−179.9
$C_3–C_4–C_8–C_{11}$	−0.348	−0.515	−0.282	$C_1–O_{15}–C_{16}–O_{17}$	1.155	0.0161	1.5777
$C_3–C_4–C_8–C_{18}$	177.7	177.86	177.93	$C_1–O_{15}–C_{16}–C_{23}$	−179.2	179.97	−178.8
$C_5–C_4–C_8–C_{11}$	−179.7	179.96	−179.8	$O_{15}–C_{16}–C_{23}–H_{24}$	179.8	179.96	−179.6
$C_5–C_4–C_8–C_{18}$	−1.667	−1.652	−1.677	$O_{15}–C_{16}–C_{23}–H_{25}$	−59.21	−58.91	−58.63
$C_4–C_5–C_6–C_1$	−0.214	0.1293	−0.075	$O_{15}–C_{16}–C_{23}–H_{26}$	58.80	58.880	59.283
$C_4–C_5–C_6–H_{10}$	−179.8	−179.9	−179.6	$O_{17}–C_{16}–C_{23}–H_{24}$	−0.537	−0.073	−0.141
$H_9–C_5–C_6–C_1$	−179.0	−178.7	−179.0	$O_{17}–C_{16}–C_{23}–H_{25}$	120.3	121.04	120.89
$H_9–C_5–C_6–H_{10}$	1.304	1.1583	1.315	$O_{17}–C_{16}–C_{23}–H_{26}$	−121.6	−121.1	−121.1
$C_4–C_8–C_{11}–H_{12}$	179.7	179.95	179.76				

The predicted and measured wavenumbers, infrared and Raman intensities were given in Table 3. Experimental spectra were shown in Fig. 1 (FT-IR) and Fig. 2 (FT-Raman). The total energy distributions for all fundamental vibrations were calculated using by scaled quantum mechanics (SQM) method at B3LYP/ 6-311++G(d,p) level.

The CH stretching vibration of the coumarin ring observed at 3172, 3092 and 3064 cm^{-1} for 6-methyl-4-bromomethylcoumarin [15]. These peaks measured at 3172 and 3079 cm^{-1} for 7-methyl-4-bromomethylcoumarin [16]. Similarly, 3159, 3087, 3067 and 3043 cm^{-1} peaks were assigned to the CH stretching vibration of the coumarin ring for 6 and 7-Chloro-4-bromomethylcoumarin [17]. We reported the molecular structure and vibrational spectra of some coumarin derivatives [17, 19, 28–30]. In these works, the C–H stretching vibrations of aromatic ring assigned at 3046–3109 cm^{-1} for 3-(bromoacetyl)coumarin and 3051–3120 cm^{-1} for 3-acetyl-7-methoxycoumarin [31]. Only four CH stretching modes are expected (mode nos. 72–69), and these are associated with the $C_2–H_7$, $C_6–H_{10}$, $C_5–H_9$ and $C_{11}–H_{12}$ bonds. The 3082 cm^{-1} (IR) band assigned to the ν_{CH} vibration. The counter part of the FT-Raman spectrum at 3071 and 3085 cm^{-1} are attributed to C–H stretching vibration. These modes are predicted by SQM procedure as pure modes.

The vibration of the bromomethyl group connected with coumarin ring is well known and described in numerous publications [15–17]. The CH_2 stretching vibrations of bromomethyl group were observed at 2987 and 2925 cm^{-1} for 6-Chloro-4-bromomethylcoumarin and at 2977 and 2926 cm^{-1} for 7-Chloro-4-bromomethylcoumarin, respectively. Sortur et al. observed that 3046 and 2963 cm^{-1} (FT-Raman) were assigned to the CH_2 stretching vibrations of bromomethyl group for 7-methyl-4-bromomethylcoumarin. In the present work, these modes (mode nos. 68 and 65) measured at 3046 cm^{-1} (3041 cm^{-1} for FT-IR) in the FT-Raman spectra as asymmetric stretching vibration. The other stretching vibration

Table 3. Calculated vibrational wavenumbers (cm^{-1}), measured FT-IR and FT-Raman bands and assignments for 7A4BMC

Normal modes	Theoretical (B3LYP)					Experimental		TED[d] (%)
	6-311++G(d,p)			cc-PVDZ	cc-PVTZ			
	Freq[a]	[b]I_{IR}	[c]I_{Raman}	Freq[a]	Freq[a]	Exp. IR	Exp. Raman	
ν_{72}	3080	0.09	5.83	3186	3135	3082	3085	ν_{HC}(99%)
ν_{71}	3071	0.08	5.06	3130	3119		3071	ν_{HC}(99%)
ν_{70}	3060	0.02	6.61	3117	3110			ν_{HC}(99%)
ν_{69}	3056	0.35	2.53	3113	3106			ν_{HC}(99%)
ν_{68}	3036	0.11	2.47	3086	3082	3041	3046	ν_{HC}(99%)
ν_{67}	3018	0.82	4.97	3081	3066	2995	2996	ν_{HC}(100%)
ν_{66}	2973	0.53	5.94	3032	3020		2938	ν_{HC}(99%)
ν_{65}	2973	0.36	3.84	3017	3018			ν_{HC}(100%)
ν_{64}	2915	0.09	13.7	2964	2962	2899	2903	ν_{HC}(100%)
ν_{63}	1767	31.3	2.74	1781	1776	1744		ν_{OC}(88%)+ ν_{CC}(5%)
ν_{62}	1744	100	47.9	1778	1757	1727	1730	ν_{CO}(85%)+ν_{CC}(6%)
ν_{61}	1602	13.1	57.9	1621	1610	1608	1614	ν_{CC}(64%)
ν_{60}	1597	21.3	37.0	1613	1605			ν_{CC}(67%)+ δ_{HCC}(10%)
ν_{59}	1538	10.4	62.3	1548	1545	1566	1567	ν_{CC}(78%)
ν_{58}	1482	1.22	8.84	1487	1492	1505	1508	δ_{HCC}(41%)+ ν_{CC}(39%)
ν_{57}	1441	2.07	2.54	1417	1448	1464	1463	δ_{HCH}(55%)+ δ_{HCC}(23%)+τ_{HCCC}(18%)
ν_{56}	1426	1.31	2.86	1413	1432			δ_{HCH}(57%)+ τ_{HCCO}(24%)+δ_{HCC}(13%)
ν_{55}	1422	2.00	2.94	1401	1428	1413	1424	δ_{HCH}(58%)+ τ_{HCCO}(28%)+δ_{HCC}(12%)
ν_{54}	1400	3.10	2.81	1395	1410	1396	1397	ν_{CC}(35%)+ δ_{HCC}(20%)
ν_{53}	1366	8.21	30.1	1368	1374	1363	1364	ν_{CC}(33%)+ δ_{HCH}(33%)
ν_{52}	1355	10.1	2.41	1340	1361			δ_{HCH}(47%)+δ_{HCC}(46%)
ν_{51}	1316	1.54	28.2	1335	1320	1323	1327	ν_{CC}(81%)
ν_{50}	1247	3.54	4.34	1254	1257	1261	1268	δ_{HCC}(58%)+ν_{CC}(15%)+ ν_{OC}(10%)
ν_{49}	1239	9.19	9.32	1241	1248	1232	1237	ν_{CC}(32%)+ ν_{OC}(26%)+ δ_{HCC}(15%)
ν_{48}	1212	4.87	26.5	1201	1215		1211	δ_{HCC}(32%)+ ν_{OC}(28%)+ν_{CC}(15%)+ δ_{HCBr}(10%)
ν_{47}	1199	2.35	2.19	1190	1199			δ_{HCC}(44%)+ δ_{HCBr}(21%)+ τ_{HCCC}(16%)
ν_{46}	1165	84.2	15.5	1179	1175	1197	1194	δ_{HCC}(37%)+ ν_{CO}(15%)+ ν_{CC}(11%)+ δ_{OCC}(11%)
ν_{45}	1156	10.5	49.5	1159	1165		1152	δ_{HCC}(48%)+ δ_{HCBr}(21%)+ν_{CC}(16%)
ν_{44}	1126	5.70	54.7	1129	1133	1147	1138	ν_{CC}(47%)+ δ_{CCC}(12%)
ν_{43}	1116	11.5	6.46	1112	1122	1122		δ_{CCH}(27%)+ν_{CC}(26%)+ ν_{OC}(16%)
ν_{42}	1094	31.7	9.87	1095	1102			δ_{HCC}(41%)+ν_{CC}(22%)
ν_{41}	1035	1.70	10.9	1039	1041	1058		δ_{HCBr} (43%)+ ν_{OC}(15%)+ δ_{HCC}(15%)
ν_{40}	1029	1.38	1.00	1017	1035	1043		δ_{HCC}(56%)+ τ_{HCCO}(35%)
ν_{39}	990	28.4	2.77	992	996	993		δ_{HCC}(32%)+ν_{CC}(18%)+ ν_{OC}(14%)
ν_{38}	972	1.87	2.47	970	978	962		δ_{HCC}(21%)+ ν_{CC}(20%)+ ν_{OC}(19%)
ν_{37}	928	0.39	0.12	954	944			γ_{HCC}(90%)
ν_{36}	890	3.24	5.27	894	898	912		ν_{CO}(30%)
ν_{35}	877	2.11	5.34	874	887	877		γ_{HCC}(15%)+γ_{OCH}(11%)+ τ_{HCCO}(10%)

Table 3. (Contd.)

Normal modes	Theoretical (B3LYP)					Experimental		TED[d] (%)
	6-311++G(d,p)			cc-PVDZ	cc-PVTZ			
	Freq[a]	[b]I_{IR}	[c]I_{Raman}	Freq[a]	Freq[a]	Exp. IR	Exp. Raman	
ν_{34}	860	4.82	3.01	869	875	865		$\gamma_{OCH}(34\%)+\gamma_{HCC}(33\%)$
ν_{33}	849	0.29	5.31	859	863	855		$\gamma_{CCH}(14\%)+\gamma_{OCH}(14\%)+\tau_{HCCO}(13\%)+\nu_{CO}(12\%)$
ν_{32}	834	5.14	0.82	836	841	824		$\nu_{CC}(16\%)+\delta_{CCC}(10\%)+\tau_{CCCH}(10\%)$
ν_{31}	798	2.17	2.58	828	816	799		$\nu_{CO}(25\%)+\nu_{CC}(12\%)+\tau_{OCCH}(10\%)$
ν_{30}	773	0.35	13.0	773	781	753		$\gamma_{HCC}(35\%)+\gamma_{HCO}(15\%)+\gamma_{CCH}(11\%)$
ν_{29}	725	0.15	7.42	750	753	738		$\nu_{CC}(17\%)+\nu_{OC}(13\%)+\delta_{CCO}(10\%)$
ν_{28}	716	0.31	0.87	722	724	712		$\tau_{HCCC}(11\%)+\nu_{CC}(10\%)+\delta_{CCO}(10\%)$
ν_{27}	694	1.59	7.24	700	706	693		$\tau_{OCCC}(22\%)+\tau_{OCCH}(22\%)+\tau_{HCCC}(11\%)+\tau_{CCOC}(10\%)$
ν_{26}	678	1.16	4.68	679	684	668		$\nu_{CC}(17\%)+\delta_{OCC}(10\%)$
ν_{25}	644	0.20	14.4	657	657		657	$\delta_{CCC}(21\%)+\nu_{CC}(18\%)+\delta_{CCO}(10\%)$
ν_{24}	628	3.07	14.1	626	635	639		$\tau_{CCCC}(16\%)+\tau_{HCCC}(16\%)+\delta_{BrCC}(10\%)$
ν_{23}	593	1.12	3.16	615	602			$\nu_{BrC}(15\%)+\delta_{OCC}(14\%)+\delta_{CCC}(13\%)$
ν_{22}	569	2.10	8.35	566	573	580		$\delta_{OCO}(15\%)+\tau_{OCOC}(10\%)$
ν_{21}	565	3.69	10.0	565	569			$\tau_{HCCO}(38\%)+\delta_{HCC}(12\%)+\tau_{OCOC}(12\%)$
ν_{20}	533	0.66	11.7	535	538	547		$\delta_{CCO}(46\%)+\delta_{CCC}(10\%)+\delta_{OCO}(10\%)$
ν_{19}	492	0.12	15.4	490	496	489	511	$\delta_{CCO}(15\%)+\nu_{CC}(13\%)+\nu_{BrC}(12\%)+\delta_{OCO}(11\%)+\delta_{CCC}(10\%)$
ν_{18}	478	0.65	26.8	484	483			$\delta_{CCO}(29\%)+\delta_{CCC}(13\%)$
ν_{17}	448	0.54	11.6	457	456	439	442	$\nu_{BrC}(18\%)+\delta_{CCO}(16\%)$
ν_{16}	424	0.69	22.4	430	429	410		$\tau_{CCCC}(34\%)+\tau_{CCCH}(15\%)+\tau_{CCCO}(11\%)$
ν_{15}	390	0.20	2.22	370	392	403		$\delta_{CCC}(26\%)+\delta_{CCO}(17\%)+\delta_{COC}(10\%)$
ν_{14}	322	0.45	9.17	322	324			$\delta_{CCC}(33\%)+\delta_{CCO}(25\%)$
ν_{13}	296	0.39	3.58	299	301			$\tau_{CCCC}(19\%)+\tau_{CCCO}(15\%)+\delta_{COC}(10\%)$
ν_{12}	259	0.15	4.03	255	262			$\delta_{CCO}(17\%)+\delta_{CCC}(11\%)+\tau_{OCCC}(10\%)$
ν_{11}	249	0.06	10.3	251	253			$\tau_{OCCC}(21\%)+\tau_{COCC}(14\%)+\delta_{CCC}(10\%)$
ν_{10}	231	0.09	6.09	233	233		214	$\delta_{CCC}(27\%)+\delta_{OCC}(21\%)$
ν_{9}	190	0.59	10.5	194	194			$\tau_{CCCC}(28\%)+\tau_{OCCC}(26\%)+\delta_{BrCC}(12\%)+\nu_{BrC}(10\%)$
ν_{8}	153	0.43	2.64	139	156		107	$\delta_{COC}(29\%)+\tau_{CCCC}(12\%)+\tau_{OCOC}(10\%)$
ν_{7}	91	0.22	9.39	122	95		91	$\delta_{CCO}(19\%)+\delta_{BrCC}(14\%)+\tau_{CCCO}(12\%)+\tau_{HCCC}(10\%)$
ν_{6}	83	0.50	17.9	94	86			$\tau_{COCC}(21\%)+\tau_{OCOC}(17\%)+\tau_{CCOC}(15\%)\tau_{OCCC}(12\%)$
ν_{5}	78	0.07	10.1	90	81			$\tau_{HCCO}(43\%)+\tau_{OCOC}(10\%)+\tau_{CCOC}(10\%)$
ν_{4}	59	0.13	17.6	69	64			$\tau_{HCCO}(45\%)+\tau_{CCOC}(10\%)$
ν_{3}	46	0.06	54.8	50	48			$\tau_{BrCCC}(22\%)+\tau_{CCCC}(14\%)+\tau_{CCCO}(10\%)$
ν_{2}	38	0.37	61.8	39	40			$\tau_{BrCCC}(34\%)+\tau_{HCCC}(11\%)+\tau_{CCOC}(10\%)$
ν_{1}	24	0.19	100	13	24			$\tau_{COCC}(88\%)$

[a]Obtained from the wave numbers calculated at 0.967 for 6-311++G(d,p)), 0.970 for cc-pVDZ, 0.965 for cc-pVTZ. ν: stretching, δ: in-plane bending, γ: out-of plane bending, τ: torsion

[b,c]Relative absorption intensities and relative Raman intensities normalized with highest peak absorption equal to 100.

[d]Total energy distribution calculated at B3LYP/6-311++G(d,p) level of theory. Only contributions more than 10% are listed.

could not be measured by means of experimental techniques.

The C–Br stretching vibration coupled with the CCO bending vibration is assigned to a weak absorption at 489 cm^{-1} in the FT-IR spectra. This peak measured at 511 cm^{-1} in the FT-Raman spectra. The band measured at 1058 cm^{-1} in FT-IR is assigned to the CH_2Br deformation vibration.

The CH_2Br deformation vibration predicted at 1035 cm^{-1} with infrared intensity of 1.7 km/mol by using B3LYP/6-311++G(d,p). It has been mixed mode with OC stretching and CCH in-plane bending vibrations. Coupled CH_2Br and C–H deformation vibration (mode no. 47) are predicted at 1199 cm^{-1}. It couldn't be measured by experimental techniques. Similarly, absorptions at 1152 cm^{-1} (FT-Raman) are assigned to the mixed CH_2Br and C–H deformation vibration (mode no. 45).

A measured band at 1464 (FT-IR) and 1463 cm^{-1} (FT-Raman) is assigned to the CH_2 scissoring vibration. It is predicted at 1441 cm^{-1} by using B3LYP/6-311++G(d,p). CH_2 rocking of bromomethyl group was detected at 1363 cm^{-1} (1364 cm^{-1} for FT-Raman) in the FT-IR spectra. The bands measured at 1211 cm^{-1} with corresponding FT-IR band was assigned to the CH_2 wagging vibration in FT-Raman spectra. CH_2 twisting vibration was observed at 1122 cm^{-1} in FT-IR spectra. As seen in Table 3, some CH_2 bending vibrations were calculated by theoretical approach. Some of them are mixed modes of CCH, ring deformation, CC, CO stretching vibrations.

Acetoxy group has the three peaks at the 2900–3100 cm^{-1} region. These peaks are the CH_3 stretching vibration of the Acetoxy group. Asymmetric stretching vibration of this group is observed at 3041 cm^{-1} in the FT-IR spectra (3046 cm^{-1} FT-Raman spectra). Other asymmetric stretching vibrations were not experimentally observed. But this peak predicted at 2973 cm^{-1} for the B3LYP/6-311++G(d,p) level of theory. 2899 cm^{-1} in the FT-IR and 2903 cm^{-1} in the FT-Raman peak is assigned to the symmetric CH_3 stretching vibration. It is to be noted that these peak are pure modes. The CH_3 in-plane bending vibrations were calculated at 1426 and 1422 cm^{-1} by using B3LYP/6-311++G(d,p). A band observed at 1413 cm^{-1} (1424 cm^{-1} for FT-Raman) in FT-IR spectra was assigned to the CH_3 in-plane bending vibration. Other vibration couldn't observed by experimental techniques. A predicted band at 1355 cm^{-1} with no corresponding experimental band was assigned to CH_3 symmetric bending vibration.

The rocking modes of CH_3 group were found at 1029, 990, 972 cm^{-1} for 6-311++G(d,p) basis set calculation. The bands measured at 1043, 993 and 962 cm^{-1} in FT-IR spectra.

Table 4. Theoretical and experimental ^{13}C spectra of the most stable of 7A4BMC molecule (with respect to TMS, all values in ppm)

	Theoretical (B3LYP/6-311++G(d,p))	Experimental
C_{23}	22.44	16.93
C_{18}	45.51	36.61
C_2	113.7	105.8
C_{11}	119.9	111.3
C_4	120.1	114.3
C_6	122.2	122.8
C_5	131.0	143.1
C_8	160.3	149.4
C_1	162.0	154.9
C_3	163.7	165.7
C_{22}	164.6	165.7
C_{16}	177.0	224.3

In previous papers [17, 19], the C=O stretching vibrations of the BAC were observed at 1731 cm^{-1} (bromoacetyl group) and 1746 cm^{-1} (coumarin ring) in the FT-IR spectra. These peaks of the 3-acetyl-7-methoxycoumarin molecule were appeared at 1683 cm^{-1} (3-acetyl group) and 1731 cm^{-1} (coumarin ring) in the FT-IR spectra [31]. The C=O stretching vibration of the coumarin ring were larger than those of other group (bromoacetyl or acetyl group). In the present work, the strong bands measured at 1727 cm^{-1} (coumarin ring) and 1744 cm^{-1} (acetoxy group) in the FT-IR spectra were assigned to C=O stretching vibrations.

4.3. NMR Spectra

The calculations of NMR chemical shifts are a very important advancement in quantum chemistry. For reliable calculations of magnetic properties, accurate predictions of molecular geometries are essential. Here we present an application of combined experimental ^{13}C NMR and theoretical molecular modeling approach. The ^{13}C NMR spectrum for 7A4BMC is summarized in Table 4. The experimental and calculated ^{13}C NMR chemical shifts are compared in Table 4 (the atom numbering is in line with Figs. 1 and 2).

NMR analysis has been done by using gauge independent atomic orbital (GIAO) method which is one of the most common approaches for calculating isotropic nuclear magnetic shielding tensors [32, 33] and often more accurate than those calculated with other approaches for the same basis set size [34, 35].

The observed NMR spectra were elucidated on the basis of the calculated NMR chemical shifts in DMSO

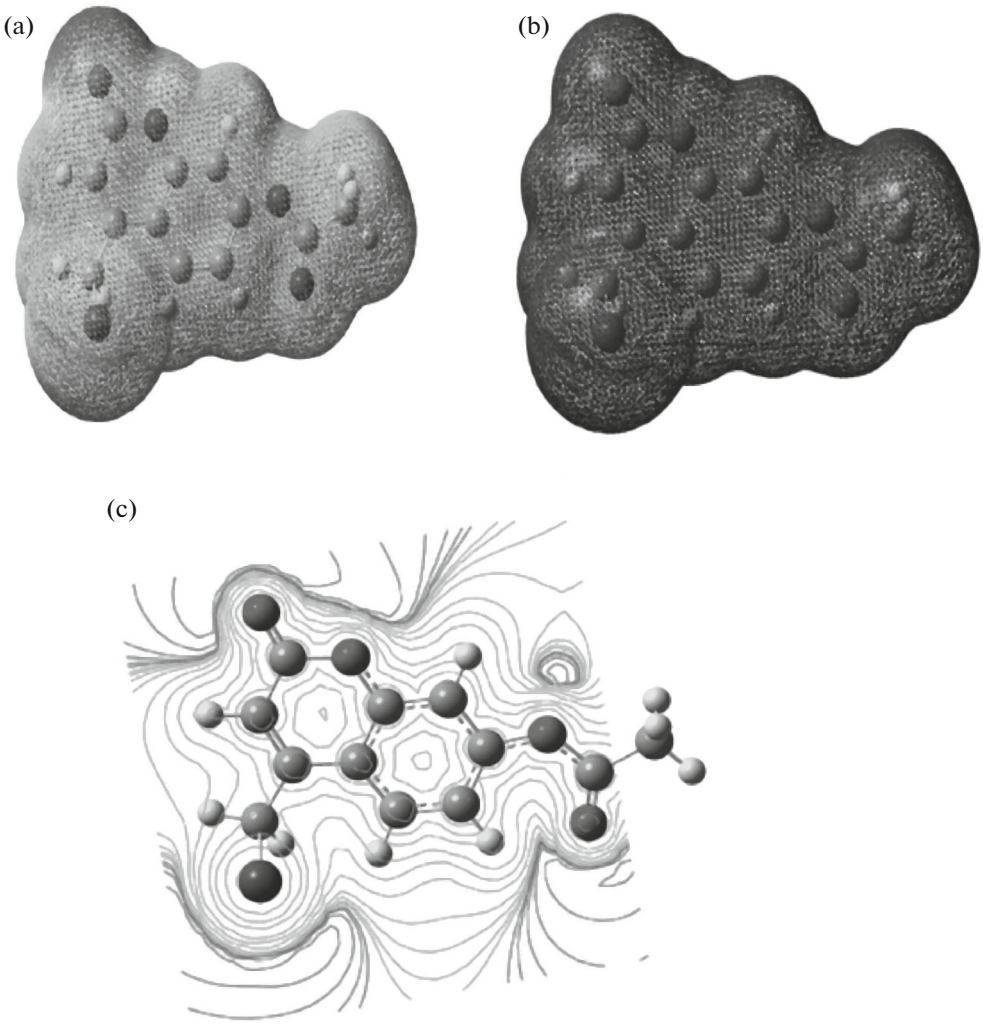

Fig. 4. (a and c) Molecular Electrostatic Potential map (b) Electron Density of 7-Acetoxy-4-(bromomethyl)coumarin compound.

for 7A4BMC. As we did our previous study, the NMR spectra calculations were performed for chloroform solvent. It is necessary to consider the solvent effects because the spectral data available are obtained in different solutions. The isotropic shielding values were used to calculate the isotropic chemical shifts δ with respect to tetramethylsilane (TMS) ($\delta_{iso}^{X} = \sigma_{iso}^{TMS} - \sigma_{iso}^{X}$) [36, 37].

Carbons of a typical organic molecule give signals in overlapped areas of the spectrum with chemical shift values from 100 to 150 ppm [38]. In this study, our molecule has twelve carbon atoms, nine carbons are in the coumarin ring, two carbon atoms are in the acetoxy group, and one carbon atom is in the bromomethyl group. The ^{13}C NMR chemical shifts of coumarin ring were measured in the 113–177 ppm region. These are clearly found in the expected regions. The computed chemical shifts as well as experimental NMR values are shown in Table 4. ^{13}C NMR spectra of the some coumarin derivatives were recorded and calculated by Zolek et al. [39].

In that study, the carbon chemical shift (in CH_3) of the acetoxy group of the 8-acetoxy-6-hydroxy-7-methoxy-4-methylocoumarin molecule was observed at 17.7 ppm. In the present paper, this chemical shift was experimentally observed at 16.938 ppm in the ^{13}C NMR spectra. This shift was predicted at 22.44 ppm by using GIAO method with IEF-PCM model. Other one was observed at 224.3 ppm by using experiment. Leon et al. found that carbon chemical shift of 3-bromomethyl-2-trifluoromethylchromone compound at 18.8 ppm by experimental approach. In that study, same chemical shift calculated at 36.0 ppm by means of B3LYP/6-311+g(2d,p). The chemical shift positions of bromomethyl group of 7A4BMC molecule lie at 36.61 ppm. This signal is predicted at 45.51 ppm by means of B3LYP/6-311++G(d,p) level of theory. Each peak identifies a carbon atom in a different envi-

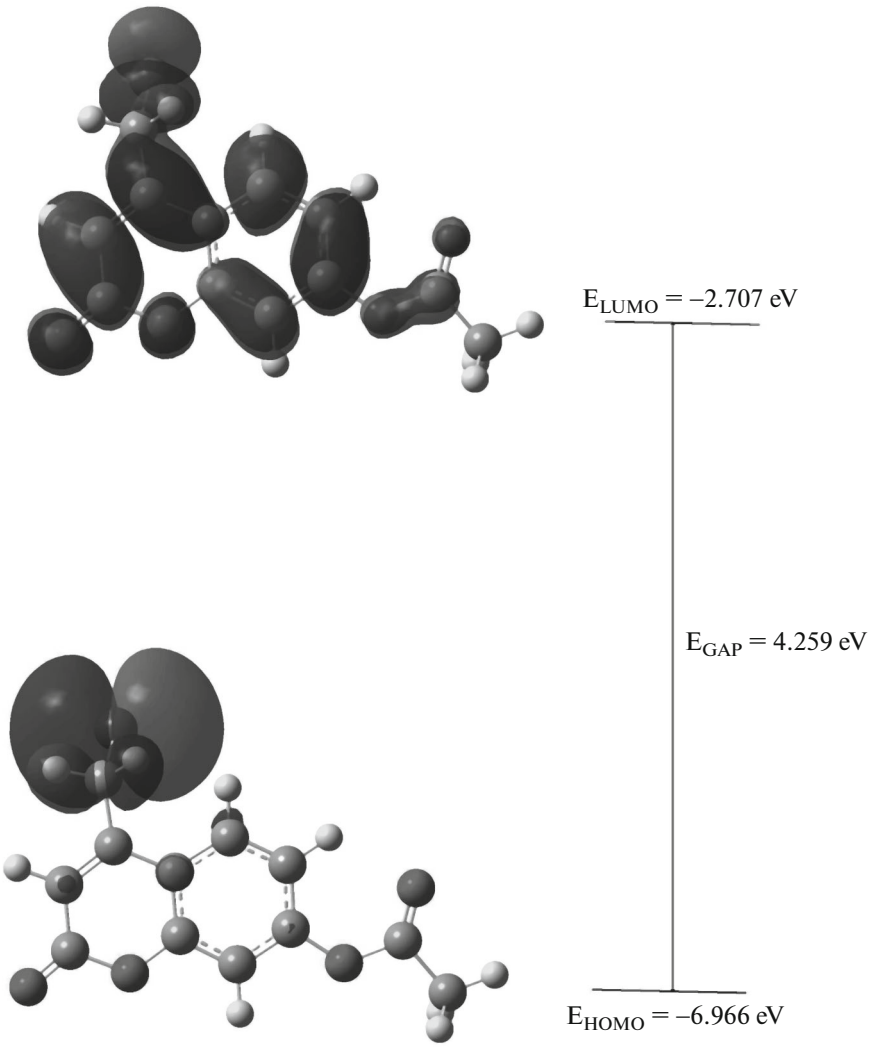

Fig. 5. HOMO and LUMO plot of 7-Acetoxy-4-(bromomethyl)coumarin compound.

ronment within the molecule. The applied magnetic field experienced by the carbon nuclei is affected by the electro negatively of the atoms attached to them.

4.4. Molecular Electrostatic Potential Maps

Because molecular electrostatic potentials (MEPs) are related to total charge distribution of a molecule, it can be used to investigate molecular interactions. Using MEPs of a molecule, it has been possible to interpret and predict the relative relativities, sites for electrophilic and nucleophilic attack, hydrogen bonding interactions. It provides correlations between chemical reactivity and the partial charges, dipole moments, electronegativity of a molecule.

The 3D plot of MEP of 7A4BMCmolecule, obtained from optimized molecular structure can be seen in Fig. 4 (color figures are available only in electronic form). It is clearly seen from this figure that while in areas susceptible to oxygen atoms are slightly positive electrostatic potential (yellow color), the regions of hydrogens of CH have sharply negative (blue color) positive electrostatic potential. Thus we can say that H regions of CH groups are the site of hydrogen bondings of our structure.

4.5. Natural Bond Orbital (NBO) Analysis

As clearly stated by Ramesh Babu the hyperconjugation may be given as stabilizing effect that arises from an overlap between an occupied orbital with another neighboring electron deficient orbital, when these orbitals are properly oriented. This non-covalent bonding (antibonding) interaction can be quantitatively described in terms of the NBO analysis, which is expressed by means of the second-order perturbation interaction energy ($E^{(2)}$) [40–44]. This energy represents the estimate of the off-diagonal NBO Fock

Table 5. Second order perturbation theory analysis of Fock matrix in NBO basis

Type	Donor (*i*)	ED, e	Acceptor (*j*)	ED, e	$E^{(2)}$, kJ/mol[a]	$E_j - E_i^c$	$F(i,j)$[b]
σ–σ*	C_1–C_2	1.971	C_1–C_6	0.028	16.61	1.27	0.064
			C_2–C_3	0.020	13.77	1.26	0.058
			C_2–H_7	0.012	6.530	1.15	0.038
			C_3–O_{14}	0.032	15.23	1.07	0.056
π–π*	C_1–C_2	1.680	C_3–C_4	0.435	95.35	0.28	0.074
			C_5–C_6	0.296	69.08	0.30	0.063
σ–σ*	C_3–C_4	1.971	C_2–C_3	0.020	17.41	1.25	0.065
			C_4–C_5	0.023	15.19	1.23	0.060
			C_4–C_8	0.034	13.89	1.20	0.056
π–π*	C_3–C_4	1.602	C_1–C_2	0.348	68.62	0.29	0.062
			C_3–C_4	0.435	6.110	0.28	0.018
			C_5–C_6	0.296	83.68	0.30	0.071
			C_8–C_{11}	0.169	69.45	0.30	0.067
σ–σ*	C_5–C_6	1.971	C_1–C_6	0.028	11.92	1.26	0.054
			C_1–O_{15}	0.039	18.95	1.03	0.061
π–π*	C_5–C_6	1.700	C_1–C_2	0.348	93.26	0.28	0.072
			C_3–C_4	0.435	71.38	0.28	0.063
σ–σ*	C_8–C_{11}	1.976	C_4–C_5	0.023	12.47	1.28	0.055
			C_4–C_8	0.034	13.97	1.24	0.058
π–π*	C_8–C_{11}	1.802	C_3–C_4	0.435	44.10	0.30	0.054
			O_{13}–C_{22}	0.276	90.96	0.30	0.074
			C_{18}–Br_{21}	0.036	29.83	0.32	0.045
σ–σ*	C_{11}–H_{12}	1.975	C_4–C_8	0.034	23.22	1.02	0.067
			O_{14}–C_{22}	0.126	18.07	0.84	0.055
σ–σ*	O_{13}–C_{22}	1.994	C_3–O_{14}	0.032	5.270	1.43	0.038
			C_8–C_{11}	0.020	2.760	1.70	0.030
π–π*	O_{13}–C_{22}	1.978	C_8–C_{11}	0.169	22.97	0.40	0.044
			O_{13}–C_{22}	0.276	3.050	0.39	0.016
σ–σ*	C_{16}–O_{17}	1.996	C_{16}–C_{23}	0.050	5.860	1.49	0.041
π–π*	C_{16}–O_{17}	1.990	C_{16}–O_{17}	0.193	2.220	0.41	0.014
σ–σ*	C_{18}–Br_{21}	1.972	C_8–C_{11}	0.020	3.640	1.19	0.029
			C_8–C_{11}	0.169	18.16	0.60	0.047

[a] $E^{(2)}$ means energy of hyper conjugative interaction (stabilization energy).
[b] Energy difference between donor (*i*) and acceptor (*j*) NBO orbitals.
[c] $F(i,j)$ is the Fock matrix element between *i* and *j* NBO orbitals.
BD*-antibonding orbital.

matrix elements. It can be deduced from the second-order perturbation approach [45, 46]:

$$E^{(2)} = \Delta E_{ij} = q_i \frac{F(i,j)^2}{\varepsilon_j - \varepsilon_i}, \quad (1)$$

where q_i is the donor orbital occupancy, ε_i and ε_j are diagonal elements (orbital energies) and $F(i,j)$ is the off-diagonal NBO Fock matrix elements. NBO analysis of FMPVH has been performed in order to explain the intra-molecular charge transfer and delocalization

of π-electrons. The intra-molecular hyperconjugative interaction is due to the overlap between π(C–C) and π*(C–C) orbitals, which results in intra-molecular charge transfer, appeared in the molecular system [40].

In the present study, the NBO analysis, which deals the intra-molecular charge transfer within the molecule, has been carried out with B3LYP/6-311++G(d,p) level of theory. The most important interactions between filled (donors) Lewis-type NBO and empty (acceptors) non-Lewis NBOs are reported in Table 5. In any molecule, the π-character of the bond plays an important role when compare with σ-bond character. In the present study, the interactions between σ- and π-bond were investigated. The electron density (ED) of donor bonds was increases whereas ED of acceptor bonds was decreases. It is evident from our study, the ED of donorbonds C_1–C_2, C_1–C_6 and C_3–C_4 are calculated about 1.971, 1.977 and 1.971e, on the other hand ED of acceptor bond and its hyperconjugation energy decreases. Similarly, the ED of π-bonds decreases with increasing ED of acceptor bond. The interaction between π–π* transition reveals maximum delocalization on contrary the σ–σ* transition reveals minimum delocalization.

4.6. Frontier Molecular Orbital Analysis

The energies of highest occupied molecular orbital (HOMO), lowest unoccupied molecular orbital (LUMO), which are very important parameters for quantum chemistry, and their energy gap, which reflects the chemical activity of the molecule, were calculated using B3LYP/6-311++G** method in this study. The calculated eigen values of LUMO and HOMO are –2.707 and –6.966 eV, respectively, while their energy gap is 4.259 eV. The plot of HOMO and LUMO are illustrated in Fig. 5.

As it is seen in Fig. 5, the region of LUMO spread over the entire molecule, while the region of HOMO overlapped in the bromomethyl group part. This indicates the charge transfer between the bromomethyl group and whole molecule through the C–C bond.

5. CONCLUSION

A systematic study has been conducted on the structural and spectral characteristics of 7A4BMC molecule by experimental spectroscopic methods and quantum chemical calculations. It shows reasonable agreement with the experimental spectra. MEP contour has been plotted in order to predict sites and relative reactivity toward electrophilic attack. The results of the NBO and the frontier orbital analysis imply an ICT in the molecule.

ACKNOWLEDGMENTS

Computing resources used in this work were provided by the National Center for High Performance Computing of Ahi Evran University (AHILAB).

REFERENCES

1. C. Ranjith, K. K. Vijayan, V. K. Praveen, and N. S. S. Kumar, Spectrochim. Acta A **75**, 1610 (2010).
2. Y. G. Sıdır and Isa Sıdır, Spectrochim. Acta A **102**, 286 (2013).
3. L. Arleth, R. Bauer, H. Ogendal, S. U. Egelhaaf, P. Schurtenberger, and J. S. Pederson, Langmuir **19**, 4096 (2003).
4. A. Chandra and B. Bagchi, Adv. Chem. Phys. **80**, 1 (1990).
5. M. Glasbeek and H. Zhang, Chem. Rev. **104**, 1929 (2004).
6. R. Giri and M. M. Bajaj, Curr. Sci. **62**, 522 (1992).
7. M. K. Subramanian, P. M. Anbarasan, and S. Manimegalai Pramana, J. Phys. **74**, 845 (2010).
8. J. Tonannavara, J. Yenagi, V. Sortur, V. B. Jadhav, and M. V. Kulkarni, Spectrochim. Acta A **77**, 351 (2010).
9. K. Bahgat, Central Eur. J. Chem. **4**, 773 (2006).
10. N. Udaya Sri, K. Chaitanya, M. V. S. Prasad, V. Veeraiah, and A. Veeraiah, Spectrochim. Acta A **97**, 728 (2012).
11. V. Arjunan, R. Santhanam, S. Sakiladevi, M. K. Marchewka, and S. Mohan, J. Mol. Struct. **1037**, 305 (2013).
12. E. Karakas Sarikaya and Ö. Dereli, J. Mol. Struct. **1052**, 214 (2013).
13. E. Karakas Sarikaya, Ö. Dereli, Y. Erdogdu, and M. T. Gulluoglu, J. Mol. Struct. **1049**, 220 (2013).
14. E. Karakas Sarikaya and Ö. Dereli, Opt. Spectrosc. (in press).
15. V. Sortur, J. Yenagi, J. Tonannavar, V. B. Jadhav, and M. V. Kulkarni, Spectrochim. Acta A **64**, 301 (2006).
16. V. Sortur, J. Yenagi, J. Tonannavar, V. B. Jadhav, and M. V. Kulkarni, Spectrochim. Acta A **71**, 688 (2008).
17. J. Tonannavar, J. Yenagi, V. Sortur, V. B. Jadhav, and M. V. Kulkarni, Spectrochim. Acta A **77**, 351 (2010).
18. M. Arivazhagan, K. Sambathkumar, and S. Jeyavijayan, Indian J. Pure Appl. Phys. **48**, 716 (2010).
19. D. Sajan, Y. Erdogdu, R. Reshmy, Ö. Dereli, K. K. Thomas, and I. Hubert Joe, Spectrochim. Acta A **82**, 118 (2011).
20. P. Hohenberg and W. Khon, Phys. Rev. **136**, 864 (1964).
21. A. D. Becke, J. Chem. Phys. **98**, 5648 (1993).
22. C. Lee, W. Yang, and R. G. Parr, Phys. Rev. B **37**, 785 (1988).
23. Spartan 10, Wavefunction Inc., Irvine, CA 92612, USA, 2010.
24. M. J. Frisch et al., Gaussian 09, Revision B. 01, Gaussian Inc., Wallingford CT, 2010.
25. H. B. Schlegel, J. Comput. Chem. **3**, 214 (1982).
26. G. Rauhut and P. Pulay, J. Phys. Chem. **99**, 3093 (1995).

27. D. Michalska, *Paint Program* (Univ. Technol., Wroclaw, 2003).
28. H. Ozisik, S. Saglam, and S. H. Bayari, Struct. Chem. **19**, 41 (2008).
29. S. H. Bayari, B. Seymen, H. Ozisik, and S. Saglam, J. Mol. Struct. Theochem **893**, 17 (2009).
30. T. R. Sertbakan, S. Saglam, E. Kasap, and Z. Kantarci, J. Mol. Struct. **482**, 75 (1999).
31. D. Sajan, R. Reshmy, K. K. Thomas, Y. Erdogdu, and I. Hubert Joe, Spectrochim. Acta A **99**, 234 (2012).
32. R. Ditchfield, J. Chem. Phys. **56**, 5688 (1971).
33. K. Wolinski, J. F. Hinton, and P. Pulay, J. Am. Chem. Soc. **112**, 8251 (1990).
34. N. Azizi, A. A. Rostami, and A. Godarzian, J. Phys. Soc. Jpn. **74**, 1609 (2005).
35. M. Rohlfing, C. Leland, C. Allen, and R. Ditchfield, Chem. Phys. **87**, 1 (1984)
36. I. Alkorta and J. J. Perez, Int. J. Quant. Chem. **57**, 123 (1996).
37. Y. Erdogdu, Spectrochim. Acta A **106**, 25 (2013).
38. M. T. Güllüoglu, Y. Erdogdu, J. Karpagam, N. Sundaraganesan, and Ş. Yurdakul, J. Mol. Struct. **990**, 14 (2011).
39. T. Zolek, K. Paradowska, and I. Wawer, Sol. St. Nucl. Magn. Reson. **23**, 77 (2003).
40. C. Ravikumar, I. Huber Joe, and V. S. Jayakumar, Chem. Phys. Lett. **460**, 552 (2008).
41. A. E. Reed and F. Weinhold, J. Chem. Phys. **78**, 4066 (1983).
42. A. E. Reed and F. Weinhold, J. Chem. Phys. **83**, 1736 (1985).
43. A. E. Reed, R. B. Weinstock, and F. Weinhold, J. Chem. Phys. **83**, 735 (1985).
44. J. P. Foster and F. Wienhold, J. Am. Chem. Soc. **102**, 7211 (1980).
45. J. Chocholousova, V. V. Spirko, and P. Hobza, Phys. Chem. Chem. Phys. **6**, 37 (2004).
46. N. Ramesh Babu, S. Subashchandrabose, M. Syed Ali Padusha, H. Saleem, and Y. Erdogdu, Spectrochim. Acta A **120**, 314 (2014).